COMPARISON OF ANATASE AND RUTILE TiO_2 NANOSTRUCTURE FOR GAS SENSING APPLICATION

S. A. HAMDAN*, I. M. IBRAHIM, I. M. ALI
University of Baghdad, College of Science, Physics Department, A-Jadiriyah, Iraq.

In this work, anatase and rutile titanium dioxide (TiO_2) phase nanostructure have been prepared with the use of the hydrothermal approach using titanium tetrachloride solution ($TiCl_3$). X-ray diffraction (XRD) results of TiO_2 were proved the anatase and rutile phases observed in the films. The measurements of the Hall effects definite that the electrons have been predominant charges in the process of the conduction (which is the n-type). The morphologies of TiO_2 nanoparticles has been observed by the Field Emission Scanning Electron Microscopy (FESEM) reveal the TiO_2 rutile films nanoflower like structure, while the TiO_2 anatase films consist of voids and particles like spherical in shape. The sensitivity of the sensors was determined by varying the conductivity of the sensor material under H_2S gas with several working temperatures. It was determined that the fabricated sensor using rutile TiO_2 nanoparticle has high sensitivity, long response time, and fast recovery time compared to anatase TiO_2 nanoparticle. Fabricated sensor based rutile TiO_2 nanoparticle has higher sensitivity at 373 °K.

(Received May 23, 2020; Accepted October 6, 2020)

Keywords: Titanium dioxide nanostructure, Anatase, Rutile, Gas sensors, H_2S gas

1. Introduction

It is well known that Titanium dioxide TiO_2 exists in 3 forms of minerals: rutile, anatase, and brookite. Anatase kind TiO_2 has a structure of crystalline, corresponding to tetragon system (with the di-pyramidal habits). The Rutile Titanium dioxide kind as well has tetragon crystal structure (with the prismatic habits). Brookite kind Titanium dioxide is of an orthorhombic crystalline structure. The Titanium dioxide is one of the multipurpose materials which have applications in different products like sunscreen lotions, paint pigments, capacitors, electro-chemical electrodes, toothpastes, solar cells, [1], photovoltaic [2], photocatalysis [3], sensors, [4] and so on. The Titanium dioxide is a wide band-gap semiconductor with a 3eV-3.20eV energy. Functional Titanium dioxide characteristics are affected with a number of the factors, such as, particles size, phase composition, preparation technique, and surface area [5]. For the purpose of producing the particles of TiO_2, a wide variety of numerous procedures of preparation like the procedure of sol-gel [6], solution combustion [7], micro-emulsion [8], chemical vapor deposition [9], and hydrothermal process [10].

The purpose of this research is utilizing hydrothermal method for synthesis of TiO_2 rutile and anatase phases nanoparticles using $TiCl_3$. Their characterization and gas sensing characteristics have been investigated. The gas sensors have been investigated as a detector for the reduction of the gas H_2S.

TiO_2 gas sensors are characteristic resistant-type sensors which can show a decrease or increase in resistance when probing a reductive gas or oxidative gas respectively [11, 12]. The hydrothermal technique has numerous benefits, such as the creation of a very homogeneous product of the crystalline that may be directly obtained at rather lower temperature of reaction. Its most important characteristic is that decreasing of the agglomeration between the particles, controlled particle morphology, and phase homogeneity. It as well provides uniform structure, mono dispersed particles, product purity, and control over the particles' size and shape [13].

* Corresponding author: suhadah22@gmail.com

2. Experimental

TiO_2 anatase phase thin films were prepared using the hydro-thermal approach. Initially, 0.1 mM of PVP dissolve in 50ml of distilled water and stirred for 30min. Na_2SO_4 0.945M dissolved in 20ml of distilled water. 0.921M of $TiCl_3$ in 10 ml of distilled water and stirred for 30 min then add PVP gradually, mix the mixture for one hour then add Na_2SO_4 the color is purple but after color change to yellow, stay on the sterrier for two hours. The mixture placed in a sealed teflon-lined autoclave reactor then annealing at 473^oK for 3 hour. The mixture has been centrifuged and then washed by distilled water, this procedure has been frequent for 3 times, then with ethanol once and dried at room temperature.

TiO_2 rutile phase synthesized using hydrothermal method. Initially, dissolve 0.3002M of NH_2CONH_2 (urea) with 20ml of distilled water and stirred for one hour at 323^oK. 4 ml of $TiCl_3$ dissolve in 20 ml of distilled water (the acidic test is 1%) and the solution stirred and add to urea. Mix the mixture for half an hour at 300 ^oK, then transferred into autoclaves and placed in the oven for five hours at 328 ^oK. The mixture has been centrifuged and washed by distilled water, this process has been repeated for three times, then with ethanol once.

The prepared TiO_2 deposited on silicon n-type (111) and glass substrate using spin coating technique. The spin parameter was 1500 rpm for 1 minute. After deposition on the substrates was dried at 373°C in order to ensure the entire residual solvent removal.

The structure of the TiO_2 anatase and rutile phase's nanostructures has been analysis and record intensity as a Bragg angle function by X–ray diffractometric system Shimadzu 6,000. The radiation source has been the Cu (Kα) with λ= 1.5405 Å wave-length, the current has been 30mA and voltage has been 40kV. The angle of the scanning 2θ has been ranged between (20^0 and 80^0) with speed 4 (degree per minute) with a preset time equal to 0.24sec.

FESEM is utilized for examining the morphology of two phases anatase and rutile TiO_2 at different rate solutions deposited on Si substrate were carried out using (MIRA3model-TE-SCAN, (Dey Petronic Co.).

The topography surface analysis has been conducted by an atomic force microscope (AFM) (AA-3000 Scanning Probe Microscope SPM, tip NSC-35/AIBS from the Angstrom Ad-Vance Inc), the micrographs of the AFM can give information on the deposit roughness on nano-metric scales, existence of the particulates and morphology of two phases anatase and rutile TiO_2 at different rate solutions deposited on glass substrate.

Hall Effect is a rich information source on conduction characteristics of the semi-conductors. The measurements of the Hall effect were performed by Van der Pauw (Ecopia HMS3000) Hall measurement systems using (0.55 Tesla) magnetic field.

3. Results and discussion

3.1. X–ray diffraction analysis

Fig. (1a) shows XRD patterns of prepared anatase Titanium dioxide phase nanostructures, which is agreement with standard peaks of anatase TiO_2 in the JCPDS (standard card NO. 96-900-9087). XRD patterns of rutile TiO_2 phase reveal in figure(1b), which is agreement with standard peaks of rutile TiO_2 phase in the JCPDS (standard card NO. 96-900-9084). The main peak at 25.3°, which corresponds to (101) plane according to TiO_2 anatase phase and (110) plane at 27.4^o according to the TiO_2 rutile phase.

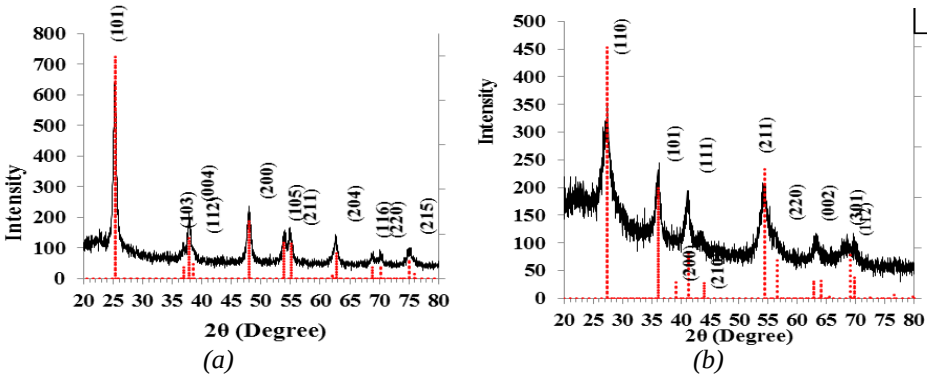

Fig. 1. The structure of (a) Anatase, (b) Rutile TiO_2 phase.

The average crystallites size (D) of TiO_2 nanostructures, with high intensity peaks for crystal planes (101) and (110) for the rutile and anatase phases respectively was estimated by Debey–Scherer's equation [14]:

$$D = k\,\lambda/\beta\,cos\theta \tag{1}$$

λ represents the Cu-Kα radiation wave-length, θ represents the angle of Bragg's diffraction, β represents full width at half maximum (FWHM) peak intensity, and *k* represents constant (approximately 0.9). Lattice constant (a, c) has been expected as well from the data of the XRD with the equation below [15]:

$$1/d_{hkl}^2 = (h^2 + k^2)/a^2 + l^2/c^2 \tag{2}$$

where (h, k, l) is the plane index of the crystal and d_{hkl}^2 is the corresponding spacing of the crystal plane. The standard and experimental interplane distances (d), FWHM, average crystallites size and Miller indices of anatase and rutile phases listed in Tables 1 and 2.

Table 1. The structural parameters for Anatase TiO_2 phase.

2θ (Deg.)	**FWHM (Deg.)**	**d_{hkl} Exp. (Å)**	**D (nm)**	**d_{hkl} Std. (Å)**	**hkl**
25.3320	0.6264	3.5131	13.0	3.5169	(101)
37.7750	0.5900	2.3796	14.2	2.3785	(004)
47.9350	0.7729	1.8963	11.2	1.8925	(200)
53.9140	1.1938	1.6992	7.5	1.7001	(105)
54.9040	0.7838	1.6709	11.4	1.6665	(211)
62.4790	0.8746	1.4853	10.6	1.4809	(204)
68.8420	0.5925	1.3627	16.3	1.3642	(116)
70.0540	0.4585	1.3421	21.2	1.3382	(220)
75.1040	1.3307	1.2639	7.5	1.2647	(215)

Table 2. The structural parameters for Rutile TiO_2 phase.

2θ (Deg.)	FWHM (Deg.)	d_{hkl} Exp. (Å)	D (nm)	d_{hkl} Std. (Å)	hkl
27.4120	1.0515	3.2510	7.8	3.2483	(110)
36.2190	0.8809	2.4782	9.5	2.4871	(101)
41.2700	0.7676	2.1858	11.1	2.1871	(111)
54.0150	0.9001	1.6963	9.9	1.6874	(211)
56.1970	0.6064	1.6355	14.9	1.6241	(220)
63.0240	0.2517	1.4738	6.46	1.4791	(002)
69.7510	0.8414	1.3472	11.5	1.3599	(301)

3.2. FESEM

FESEM images illustrates in figure (2) for the TiO_2 rutile and anatase nanoparticles at low and high magnifications. Fig. 2(a, b) reveal the rutile TiO_2 nanostructure nanoflower like structure at 200nm magnifications, while for 2(c, d) the TiO_2 particles, may be due to the synthesis method and its preparation conditions.

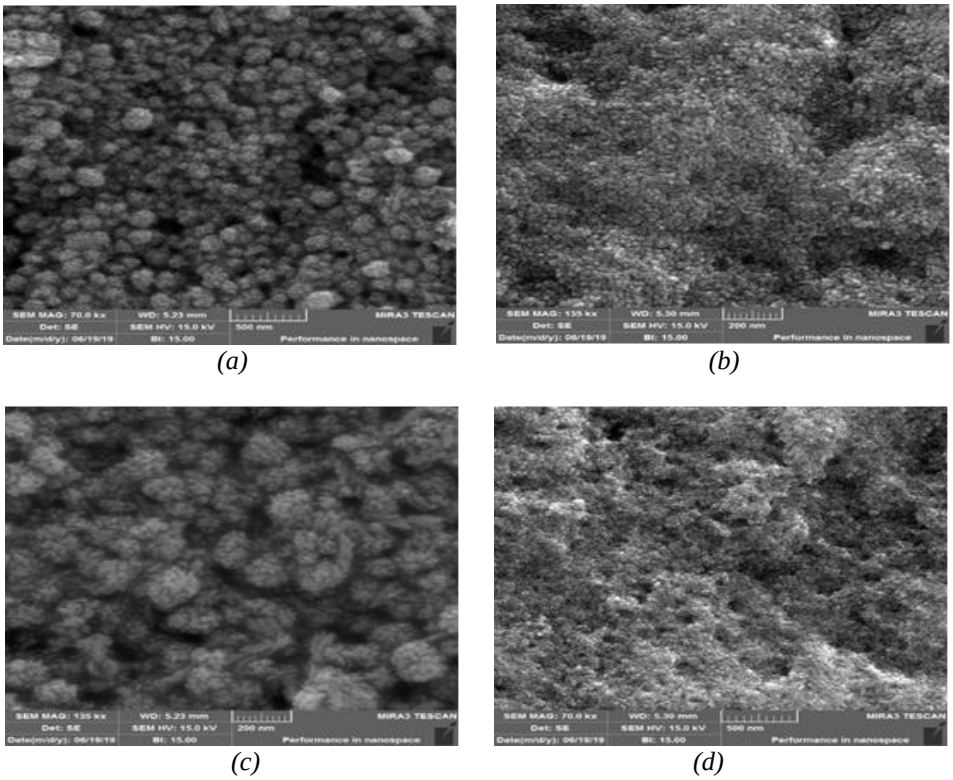

(a) *(b)*

(c) *(d)*

Fig. 2. Images of the FESEM of TiO_2 (a), (b) rutile phase and (c), (d) anatase phase.

3.3. AFM

The topography of anatase and rutile TiO2 phases were tested by AFM analysis so as to offer a large surface inspection of microstructural arrays. Figs. 3 and 4 show the images with (2D, 3D) for anatase and rutile TiO2 phase respectively.

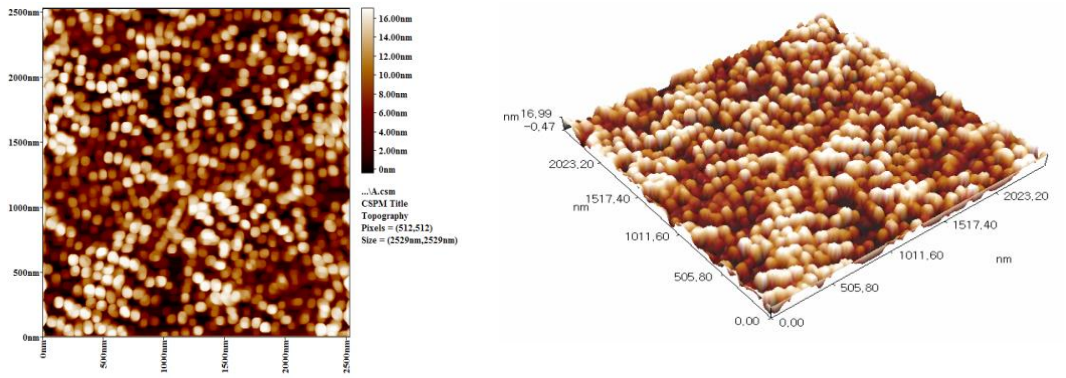

a) *b)*

Fig. 3. (a) 2-D and (b) 3-D AFM images of Anatase TiO2 nanoparticles

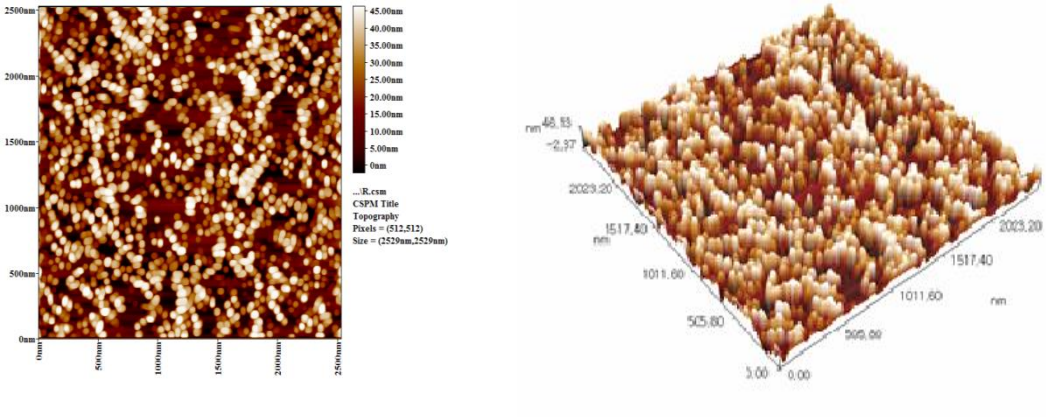

a) *b)*

Fig. 4. (a) 2-D and (b) 3-D AFM images of Rutile TiO_2 nanoparticles.

Topography parameters contain average roughness, average diameter, root mean square (RMS), and roughness for samples are tabulated as can be seen in Table 3. From the results notice rutile TiO_2 phase has small average diameter, high average roughness compare with anatase TiO_2 phase. Roughness can be generally observed as one of the significant parameters. The surface roughness not merely describes the scattering of the light, but also provides information on the quality of the studied surface.

Table 3. Grain size, Roughness average and (RMS) Roughness (nm) of deposited Anatase and rutile TiO_2 nanoparticle.

Sample	**AV.Diameter (nm)**	**AV. Roughness(nm)**	**(RMS) Roughness (nm)**
Anatase	76.37	4.37	5.04
rutile	57.32	12.1	14

4. Gas sensor

The sensing properties of TiO_2 anatase and rutile sensors deposited on n-Si are examined, as a function of time and operating temperature for finding the temperature dependence of sensitivity against reducing gas (H_2S).

Hall measurements shows that anatase and rutile TiO_2 films are of a negative hall coefficient (n-type charge carrier).

Figs. (5a) & (5b) show resistance variation as a time function with on/off gas valve for TiO_2 anatase and rutile sensors respectively, upon exposure to reducing gas H_2S with a 50ppm concentration at different operating temperature values, starting from the room temperature to 473 ^oK with gradually increase of 323^oK.

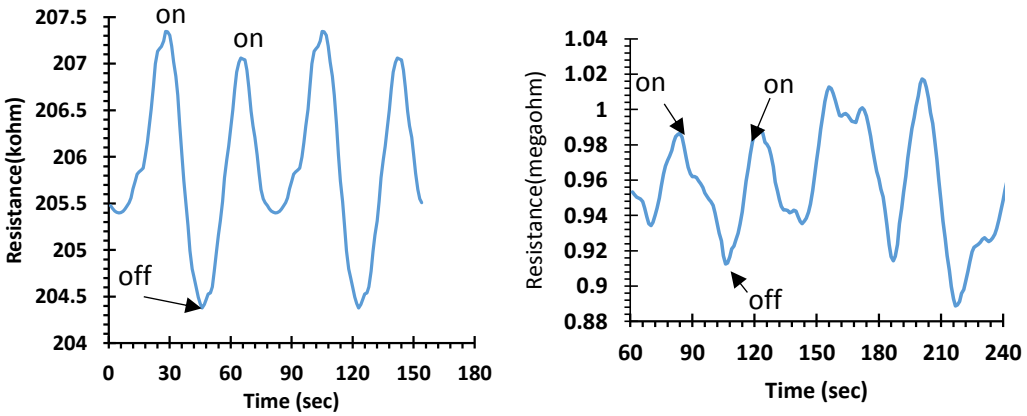

Fig. 5. Resistance as function of time for (a)anatase TiO_2 nanoparticle (b)rutile TiO_2 nanoparticle at RT.

The figures above illustrate the decrease of the values of the resistance when the films have been exposed to the H_2S gas (Gas ON), then the value of the resistance has been increased at the gas closure (Gas OFF). The reason for such behavior may be attributed to the fact that the molecules of the oxygen on the metal oxide surface gains the electrons from metal oxides and form the ions of the oxygen. The surfaces of the metal oxide have a hole layer of accumulation for p-type and layer of the electron depletion for n-type. In the case where the reductive gases have been introduced, the resistance of n-type metal oxide gas sensor decreases because of decreasing the thickness of the electron depletion layer [16, 17].

The sensitivity can be calculated as given as [18]:

$$S = |(R_g - R_a)/R_a| * 100\% \quad (3)$$

S represents sensitivity, R_a & R_g represent the film's electrical resistance in air and the existence of the gas, respectively.

The recovery time t_{rec} and the response time t_{res} can be characterized as the time which is needed for the changes in the electrical resistance to take place, from base resistance which is measured in the air or the gas to 90% of the stable signal post introducing air or gas.

The response and recovery times may be calculated as follows [19]:

$$t_{res} = |t_{gas}(on) - t_{gas}(off)| \times 0.9 \quad (4)$$

$$t_{rec} = |t_{gas}(off) - t_{gas}(on)| \times 0.9 \quad (5)$$

The response depends on the type and concentration of the gas, and the working temperature of the sensor. According to the presented results, TiO_2 anatase phase sensor response to H_2S at (RT, 373, and 473)^oK, while TiO_2 rutile phase sensor response to H_2S at (RT, 323, 373, 423, and 473)^oK as shown in figure (6), one can see high sensitivity is equal to 14.2% for TiO_2 rutile while equal to 2.6% for TiO_2 anatase at 373^oK.

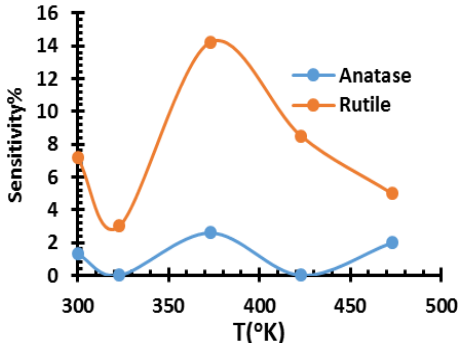

Fig. 6. Sensitivity variation with operating temperature for anatase TiO_2 and rutile sensors against H_2S gas.

TiO_2 rutile has high sensitivity because of having smaller size of the grain and higher roughness surface compare with TiO_2 anatase, as obtained TiO_2 rutile nanoflowers promote high ratio of surface-to-volume. Since it is thin film with smaller size of the grain, which is preferred as increased ratio of the surface to volume, enhanced catalytic activity, and carrier concentration facilitate its interactions with the larger amount of the gas molecules [20].

Moreover the response time significantly longer for TiO_2 rutile than TiO_2 anatase based sensors as shown in table(4), may be because the flower-like sensor's surface is of a high complexity and more advanced. The molecules of the gas require considerably more time for reaching deep in the sensor's surface structure and be adsorbed.

From results the sensor based on a TiO_2 rutile have shown the highest efficiency for reducing gas H_2S detection in contrast TiO_2 nano-structured sensor anatase agreement with Wojciech et al. [21].

Table 4. Response time and Recover time results of anatase TiO_2 and rutile thin films for H_2S gas at different operating temperature.

Operation Temp.	**RT**		**323°K**		**373°K**		**423°K**		**473°K**	
sample	$t_{Res.}$ (s)	$t_{Rec.}$ (s)	$t_{Res.}$ (s)	$t_{Rec.}$ (s)	$t_{Res.}$ (s)	$t_{Rec.}$ (s)	$t_{Res.}$ (s)	$t_{Rec.}$ (s)	$\tau_{Res.}$ (s)	$\tau_{Rec.}$ (s)
TiO_2 antase phase	5.4	14.4	-	-	17.1	13.5	-	-	13.5	13.5
TiO_2 rutile phase	16	9	21.9	10.8	32.4	13.5	27	10	13.5	5.4

5. Conclusion

In conclusion we have demonstrated, the TiO_2 nanostructures' anatase and rutile phases were prepared by hydrothermal method successfully. We compared the sensitivity of rutile and anatase phases of TiO_2. Higher sensitivity of sensor based on a TiO_2 rutile than that TiO_2 anatase, may be a result of the higher effective surface area. Longer TiO_2 rutile delay time is possibly a result of longer required time or adsorbing more oxygen molecules for reaching initial state.

Acknowledgments

This work was supported by thin film laboratories, physics Departments, Baghdad University. We acknowledge the helpful all staff assistance of this laboratories.

References

[1] G. Meacock, K. Taylor, M. Knowles, A. Himonides, J. Sci. Food. Agric. **73**, 221 (1997).
[2] J. Lin, Y.U. Heo, A. Nattestad, Z. Sun, L.Wang, J. H. Kim, S. X. Dou, Scientific reports **4**, 5769 (2014).
[3] I. Paramasivam, H. Jha, N. Liu, P. Schmuki, Small **8**, 3073 (2012).
[4] I. M. Ibrahim, S. I. Sharhan, Nano Hybrids and Composites **25**, 12(2019).
[5] M. Montazeri-Pour, N. Riahi-Noori, A. Mehdikhani, R. Sarraf-Mamoory, Proceeding of the international conference nanomaterial: applications and properties **1**(1), (2012).
[6] M. Hussain, R. Ceccarelli, D. L. Marchisio, D. Fino, N. Russo, F. Geobaldo, Chem. Engin. J. **157**, 45(2010).
[7] K. Nagaveni, M.S. Hegde, N. Ravishankar, G.N. Subbanna, G. Madras, Langmuir **20**, 2900 (2004).
[8] F. A. Deorsola, D. Vallauri, Powder Tech. **190**, 304 (2009).
[9] H. Lee, M. Y. Song, J. Jurng, Y.-K. Park, Powder Tech. **214**, 64 (2011).
[10] A. Testino, I. R. Bellobono, V. Buscaglia, C. Canevali, M. D'Arienzo, S. Polizzi, R. Scotti, F. Morazzoni, J. Amer. Chem. Soc. **129**, 3564 (2007).
[11] M. Kimura, R. Sakai, S. Sato, T. Fukawa, T. Ikehara, R. Maeda, T. Mihara, Adv. Funct. Mater. **22**, 469 (2012).
[12] J. Nisar, Z. Topalian, A. De Sarkar, L. Österlund, R. Ahuja, ACS Appl. Mater. Interfaces **5**, 8516 (2013).
[13] G. J. Mogal, G. E. Patil, F. I. Ezema, V. B. Gaikwad, Gotan H. Jain, International Journal of Enhanced Research in Science Technology & Engineering **3**(12), 86 (2014).
[14] M. Thakurdesai, N. Kulkarni, B. Chalke, A. Mahadkar, Calcogenide Letters **8**(3), 223 (2011).
[15] K. Sirohi, S. Kumar, V. Singh, A. Vohra, Acta Metallurgica Sinica(English Letters) **31**(3), 254 (2018).
[16] N. Yamazoe**,** Sensors and Actuators B: Chemical **5**, 7 (1991).
[17] S. Kannan, L. Rieth, F. Solzbacher, Sensors and Actuators B: Chemical **149**, 8 (2010).
[18] L. A. Patil, A. R. Bari, M. D. Shinde, V. V. Deo, D. P. Amalnerkar, IEEE Sens. J. **11**(12), 939 (2011).
[19] D. R.Patil, L. A.Patil, G. H. Jain, M. S. Wagh,Sensors Transducers J. **74**, 874 (2006).
[20] P. Shankar, J. B. B. Rayappan, Science Jet **4**, 126 (2015).
[21] W. Maziarz, A. Kusior and A. Trenczek-Zajac, Beilstein J. Nanotechnol **7**, 1718 (2016).